ACS APPLIED MATERIALS & INTERFACES

Research Article

www.acsami.org

Controlled Layer-by-Layer Etching of MoS_2

TaiZhe Lin,[†,∥] BaoTao Kang,[⊥] MinHwan Jeon,[‡] Craig Huffman,[§] JeaHoo Jeon,[‡] SungJoo Lee,[‡] Wei Han,[∥] JinYong Lee,[⊥] SeHan Lee,[‡] GeunYoung Yeom,*[,†,‡] and KyongNam Kim*[,†]

[†]Department of Advanced Materials Science and Engineering, Sungkyunkwan University, Suwon 440-746, Korea

[‡]SKKU Advanced Institute of Nano Technology (SAINT), Sungkyunkwan University, Suwon 440-746, Korea

[§]SEMATECH, 257 Fuller Road, Suite 2200, Albany, New York 12203, United States

[∥]Department of Physics, Jilin University, Changchun, Province of Jilin China

[⊥]Department of Chemistry, Sungkyunkwan University, Suwon 440-746, Korea

Supporting Information

ABSTRACT: Two-dimensional (2D) metal dichalcogenides like molybdenum disulfide (MoS_2) may provide a pathway to high-mobility channel materials that are needed for beyond-complementary metal-oxide-semiconductor (CMOS) devices. Controlling the thickness of these materials at the atomic level will be a key factor in the future development of MoS_2 devices. In this study, we propose a layer-by-layer removal of MoS_2 using the atomic layer etching (ALET) that is composed of the cyclic processing of chlorine (Cl)-radical adsorption and argon $(Ar)^+$ ion-beam desorption. MoS_2 etching was not observed with only the Cl-radical adsorption or low-energy (<20 eV) Ar^+ ion-beam desorption steps; however, the use of sequential etching that is composed of the Cl-radical adsorption step and a subsequent Ar^+ ion-beam desorption step resulted in the complete etching of one monolayer of MoS_2. Raman spectroscopy, X-ray photoelectron spectroscopy (XPS), and atomic force microscopy (AFM) indicated the removal of one monolayer of MoS_2 with each ALET cycle; therefore, the number of MoS_2 layers could be precisely controlled by using this cyclical etch method. In addition, no noticeable damage or etch residue was observed on the exposed MoS_2.

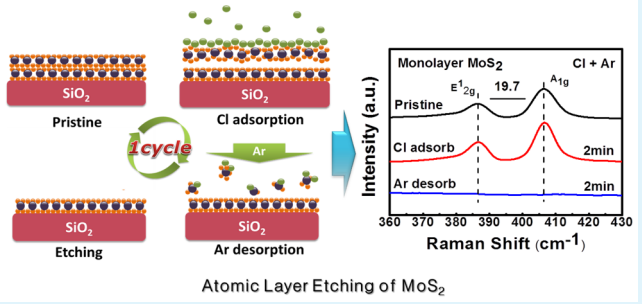

Atomic Layer Etching of MoS_2

KEYWORDS: *MoS_2, atomic layer etching, layer by layer etching, two-dimensional (2D) material, adsorption, desorption, plasma*

1. INTRODUCTION

Molybdenum disulfide (MoS_2) is a typical layer-structured composite metal dichalcogenide composed of a S−Mo−S crystal structure and is one of the newly investigated two-dimensional (2D) electronic materials that is similar to graphene.[1−7] van der Waals force is dominant between the layers, while covalent bonds control the interaction within the layers.[8−12] MoS_2 is a semiconducting material, and different band gap energies have been found for different numbers of MoS_2 layers. As the layers of material decrease, the band gap is enhanced from 1.29 to 1.8 eV (a monolayer is due to the quantum confinement effect). At the same time, with a decrease of the number of layers, a tendency from the indirect gap to the direct gap is observed between the conduction band and the valence band.

MoS_2 has a stable crystal structure, does not react with strong acids, and has an electron mobility that can reach 200 $cm^2\ V^{-1}\ s^{-1}$ at room temperature.[11,12] MoS_2-monolayer field-effect transistors that have been fabricated with hafnium(IV) oxide (HfO_2) as the gate dielectric show a current on/off ratio as high as 1×10^8 at room temperature and a very low standby-power dissipation; therefore, it can be used in the fabrication of 2D semiconductor nanodevices.[13] The volume of MoS_2 is smaller than that of an Si crystal structure, and the mass of MoS_2 is lighter than the Si crystal structure when it obtains the same electron-mobility effect. At a steady state, the energy consumption is known to be lower than that of traditional Si transistors.[14] Moreover, MoS_2 is investigated as a promising material for hydrogen evolution,[15] transistors,[16,17] and sensors,[18] in addition to flexible electronics due to a high Young's modulus of approximately 33 TPa.[19]

The electronic properties of 2D materials and their application strongly depend on the number of layers; therefore, a simple and efficient method to control thickness is necessary. The chemical vapor deposition (CVD) method is widely investigated regarding the growth of large-area MoS_2, but currently, it is difficult to control the layers of MoS_2, especially for a low layer number, with this method. At present, only MoS_2 devices that use a MoS_2 flake obtained by exfoliation have a proven reliability.[13,17]

Received: April 23, 2015
Accepted: June 19, 2015
Published: June 19, 2015

DOI: 10.1021/acsami.5b03491
ACS Appl. Mater. Interfaces 2015, 7, 15892−15897

Instead of the control of MoS_2 layers by growth, MoS_2 layers can be controlled by removing the layers after synthesis. Recently, the use of argon (Ar) plasma to conduct the layer-by-layer etching of MoS_2 has been investigated by Liu et al., and the results showed the possibility of using sputter etching to achieve a monolayer MoS_2; however, their etching process resulted in physical damage to the sample surface, as detected by Raman spectroscopy.[15,20] Huang et al. controlled the MoS_2 layer thickness by using xenon difluoride (XeF_2) etching, which formed volatile etch products such as molybdenum hexafluoride (MoF_6) and sulfur hexafluoride (SF_6) without damaging the sample.[11] Castellanos-Gomez et al. reported the use of a laser thinning technique on a multilayer MoS_2 film to achieve a monolayer, but this method showed drawbacks such as thermal damage to the bottom layer.[21] Thermal-annealing and oxygen-treatment methods have also been reported as approaches that can thin MoS_2.[14,15,22] On the basis of an analysis of all of the currently reported techniques, however, the removed MoS_2 depth can only be controlled by etch time, and a precise control of the number of MoS_2 layers at the atomic scale cannot be achieved.

Previously, in the etching of various semiconducting materials, the atomic layer etching technique (ALET) has shown promising results for next-generation devices due to characteristics such as precise atomic-scale control of the etch depth, extreme uniformity over a large wafer area, and low levels of damage and contamination.[23−26] In this research, we propose the ALET as a precise layer-by-layer etching technique for 2D MoS_2 material. Using ALET, we investigated the possibility of removing one monolayer of MoS_2 through the chemical absorption and physical desorption of the cyclic reaction. Also, the possibility of obtaining one monolayer of MoS_2 from a trilayer MoS_2 formation without inducing damage and contamination on the remaining MoS_2 layers was explored.

2. EXPERIMENTAL SECTION

The 2D MoS_2 layers that had been synthesized using the CVD method (shown in Figure S1 in Supporting Information) were etched layer by layer using a two-step ALET. First, chlorine radicals that were generated from an inductively coupled plasma (ICP) system were adsorbed onto the MoS_2 surface. Then, the chlorinated MoS_2 surface was removed using a low-energy Ar^+ ion beam.

During Cl-radical adsorption, ion bombardment was significantly reduced by installing a grounded, metal mesh grid between the ICP source and the substrate. The Cl_2 plasma for adsorption was generated with 63 sccm of Cl_2 and 18 W 13.56 MHz radio frequency (rf) source power at 10 mTorr pressure. For the desorption step, the samples were transferred to a dual-grid Ar^+ ion-beam system. The process conditions were 70 sccm of Ar, 200 W 13.56 MHz ICP power, and 6.7 mTorr pressure. An extraction grid voltage of between +10 and +100 V was used to accelerate the Ar^+ ion, while the outside grid of the ion-beam system was grounded. (For schematic diagrams of the ICP systems used for the adsorption of the Cl radical and the Ar^+-ion-beam system used to desorb the chemisorbed MoS_2 layer, see Figure S2, (a) and (b).) The ion flux and energy distribution of the Ar^+ ion beam were measured using a quadruple mass spectrometer with an ion energy analyzer (Hiden Analytical Ltd., EQP1000) that was located close to the sample location (shown in Figure S2, (b)).

The numbers of MoS_2 layers before and after the layer-by-layer etching were estimated using Raman spectroscopy (WITEC 2000, 532 nm wavelength, installed with a grating of 1800 grooves/m and a spectral center of 600 cm^{-1}). The thickness was determined by measuring the shift of the Raman peaks at the E^1_{2g} and A_{1g} peaks. The thickness of the MoS_2 was also measured using atomic force microscopy (AFM, INOVA microscope by Bruker) and a sample patterned by photoresist; the photoresist was removed before the measurement with AFM. The chemical binding states of the MoS_2 surface before and after the Cl-radical adsorption and before and after the Ar^+ ion desorption were observed using X-ray photoelectron spectroscopy (XPS, Thermo VG, Multilab 2000).

3. RESULTS AND DISCUSSION

The schematic diagram of the atomic layer etching of MoS_2 using the adsorption of Cl radicals and the desorption of Cl-adsorbed MoS_2 is shown in Figure 1. Since Cl is a better

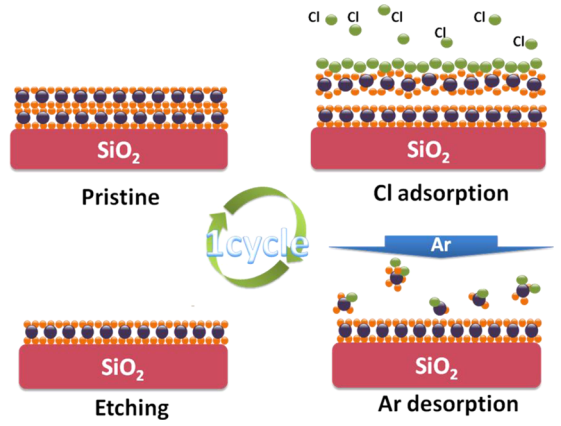

Figure 1. Schematic drawing of MoS_2 ALET cycle for the layer-by-layer etching.

oxidizing agent than S, the adsorbed Cl on the MoS_2 surface weakens the covalent bonding between the outermost electrons in Mo $4d^5 5s^1$ and S $3s^6$. The bond angle is changed and the bond length is increased by the movement of Mo electrons toward the surface Cl atom; therefore, the adsorption of Cl on MoS_2 not only changes the Mo−S binding energy but also decreases the van der Waals force between the MoS_2 layers.[27−29] The weakened Cl-adsorbed MoS_2 top layer was physically desorbed by the ion bombardment from a low-energy Ar^+ ion beam during the desorption step. The Ar^+ ion bombardment not only breaks the Mo−S binding in the layer but also removes the broken MoS-Cl/S−Cl from the MoS_2 surface. This process will continue until all of the broken MoS−Cl/S−Cl species are removed and the next MoS_2 layer is exposed.

During Cl-radical adsorption, the MoS_2 layer should not be chemically etched by the plasma etching, which involves the synergic effect of Cl-radical adsorption and Cl^+ ion bombardment. The removal of these reactive Cl^+ ions is accomplished by the grounded, metal mesh grid that was installed between the ion beam and wafer surface, as shown in Figure S2. Figure 2 shows the Raman spectra of one monolayer of MoS_2 before and after Cl-radical exposure. The monolayer MoS_2 surface was exposed to the Cl radicals for 2 and 10 min. As shown in Figure 2, for the pristine MoS_2, two peaks related to the E^1_{2g} and A_{1g} peaks of the MoS_2 crystal were observed at 386.4 cm^{-1} (in-plane vibration mode) and 406.1 cm^{-1} (out-of-plane vibration mode), respectively; therefore, the gap between the two peaks was about 19.7 cm^{-1}, indicating the monolayer MoS_2. The width of the Raman peaks of the monolayer MoS_2 that was measured after the Cl-radical exposures of 2 and 10 min was not changed; therefore, the Cl exposure did not etch the monolayer MoS_2.

During the desorption step, the weakened Cl-adsorbed MoS_2 bonds were broken and desorbed by the Ar^+ ion bombardment.

DOI: 10.1021/acsami.5b03491
ACS Appl. Mater. Interfaces 2015, 7, 15892−15897

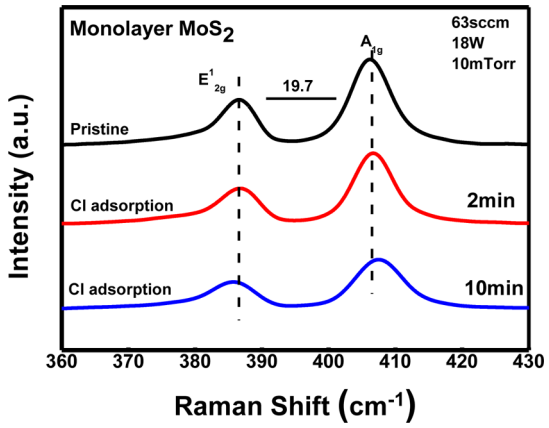

Figure 2. Raman spectra of one monolayer of MoS_2 before and after the exposure to the Cl plasma for the Cl-radical-adsorption step up to 10 min. No change in the Raman spectra of the MoS_2 was observed, even after a 10 min exposure.

Ion-energy control is critical for the desorption of the Cl-modified MoS_2 surface. If the energy is too high, then the unreacted MoS_2 is damaged; conversely, if the ion energy is too low, no amount of material is removed. During the Ar^+ ion exposure for the desorption step, the energy of the Ar^+ ion was varied to investigate the Ar^+ ion-energy window during the desorption step. Figure 3a shows the Raman spectra of the monolayer MoS_2 before and after the Ar^+ ion exposure at different grid voltages, which controls the energy of the Ar^+ ions bombarding the MoS_2 surface. As shown in the figure, when the MoS_2 was exposed to the Ar^+ ion source for 2 min with a grid voltage higher than +30 V, no Raman peaks were observed, indicating that the MoS_2 was removed. However, when the MoS_2 was exposed to the Ar^+ ion beam using a grid voltage of +10 V for 2 and 10 min, no change was observed. This indicates that there was no change to the MoS_2 material when +10 V was used to accelerate the Ar^+ ion beam. Figure 3b shows the Ar^+ ion-energy distribution that was measured using an ion-energy analyzer during the Ar^+ ion-desorption step for different grid voltages between +10 and +70 V. As shown in Figure 3b, the ion energy distribution for +10 V grid voltage showed a nearly monoenergetic Ar^+ ion beam, with an energy peak at approximately +20 eV (10−25 eV).

Figure 4 shows the Raman spectra in sequence following the previously described optimized-process step on the monolayer MoS_2 sample. For the Cl-radical adsorption step, 2 min of Cl-radical exposure time was used, and for the Ar^+ ion desorption step, 2 min exposure time with +10 V of grid voltage was used. As previously shown, no change was detected in the peak width between the pristine and Cl-exposed steps; however, when the Cl-modified MoS_2 was exposed to the Ar^+ ion-desorption step, no peaks were detected, indicating that the monolayer MoS_2 was completely removed. It is therefore expected that during the Cl-adsorption step, the MoS_2 binding energy is weakened by chlorine adsorbing onto the MoS_2 and is then removed during the desorption step by the controlled Ar^+ ion energy.

Controlled thinning of multilayer MoS_2 may be possible using the above-described process. To demonstrate, a trilayer MoS_2 sample was exposed to three cycles of ALET and Raman spectra were collected between each step. Figure 5a and Figure 5b show the Raman spectra and the peak distance between the E^1_{2g} and A_{1g} peaks, respectively, as the process progresses through each step. It is known that with a decrease of the MoS_2

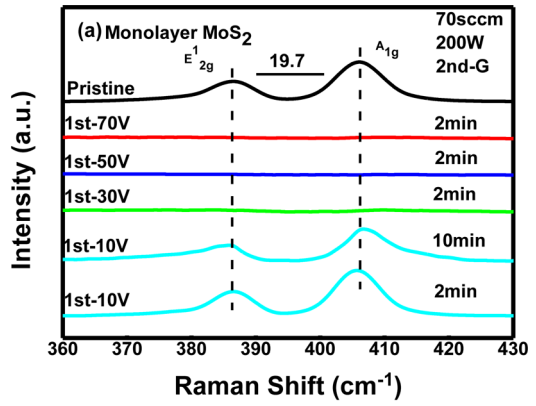

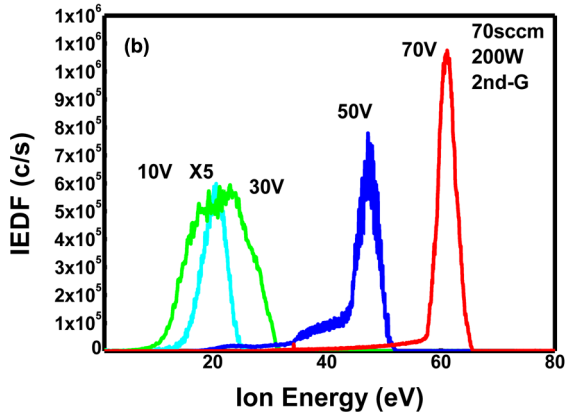

Figure 3. (a) Raman spectra of one monolayer of MoS_2 exposed to different Ar^+ ion energies for 2 min by changing the first grid voltages of the ICP ion gun. For +10 V of the first grid voltage, 10 min exposure to the Ar^+ ion beam is also included. (b) Ar^+ ion energy distribution for +10 V to +70 V of the first grid voltage measured using a quadruple mass spectrometer with an ion energy analyzer. For the Ar^+ ICP ion gun operation, 70 sccm of Ar and 13.56 MHz 200 W rf power were applied to the ICP source. "X5" means that the actual ion-energy distribution of +10 V is 5 times smaller than that shown in the figure.

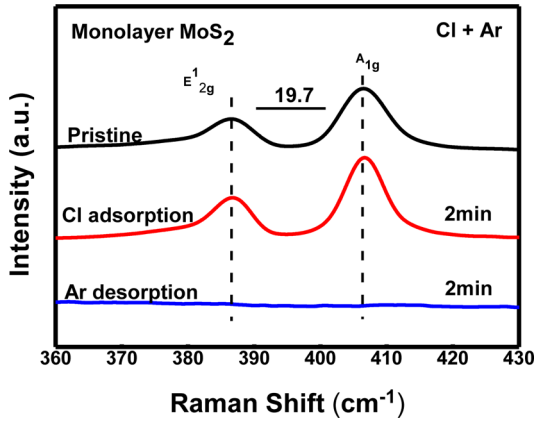

Figure 4. Raman spectra of pristine MoS_2 monolayer, after Cl_2 adsorption for 2 min, and after Ar^+ ion desorption for 2 min, sequentially, resulting in the etching of one monolayer of MoS_2.

layer thickness, the peak distance between the E^1_{2g} and A_{1g} peaks is decreased to a specific value, depending on the number of MoS_2 layers.[6,11,12,16,30] As shown in Figure 5a and Figure 5b, during the Cl-adsorption step, the peak distance does not change; however, after each Ar^+ ion-desorption step, the gap

DOI: 10.1021/acsami.5b03491
ACS Appl. Mater. Interfaces 2015, 7, 15892−15897

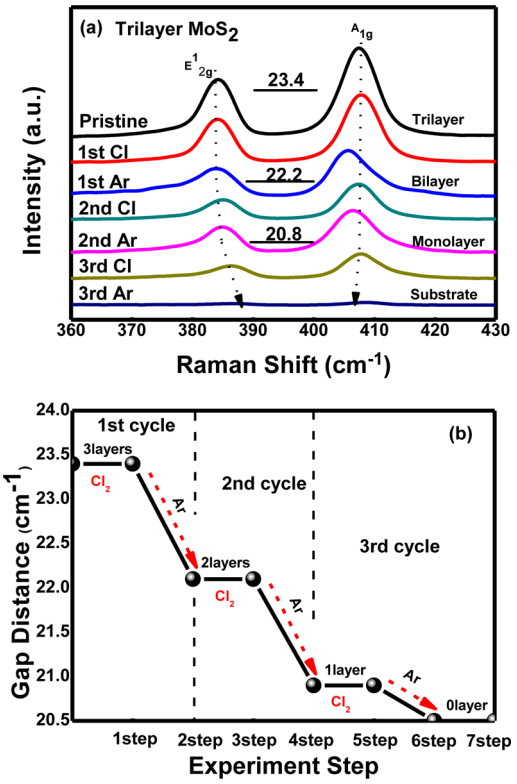

Figure 5. Raman spectra of trilayer MoS_2 after each step of ALET for three cycles: (a) Raman spectra of MoS_2 during each step of ALET; (b) change of the gap distance between E^1_{2g} and A_{1g} of the MoS_2 Raman spectra during each step of the three ALET cycles.

between the E^1_{2g} and A_{1g} peaks decreased by a specific value related to monolayer-to-bilayer MoS_2. (In addition to the CVD MoS_2, a similar ALET experiment was carried out using trilayer MoS_2 flakes obtained from crystal MoS_2. The trilayer MoS_2 was etched using the same ALET cycle, and after one ALET cycle, the peak distance decreased to the specific value related to bilayer MoS_2. See Figure S3.) Also, when the MoS_2 structure is distorted by the physical ion bombardment, the E^2_{1u} peak near 379 cm^{-1} is known to appear because of the Raman edge effect that is caused by the distortion of the MoS_2 structure,[6,16,30] but as shown in Figure 5a, no such peak was observed. It can therefore be understood that during each ALET cycle, one monolayer MoS_2 was completely removed without noticeably damaging the exposed MoS_2 underlayer.

In addition to Raman spectroscopy, the change of the MoS_2 layer during the ALET cycles was measured using AFM. For this measurement, a trilayer MoS_2 film was masked with photoresist and exposed to one and two ALET cycles. The photoresist was removed by acetone, and the step was measured using AFM. Figure 6a) and Figure 6b show the AFM data after a single cycle of ALET for the monolayer MoS_2 and two cycles of ALET for the trilayer MoS_2, respectively. As shown in Figure 6a, after one ALET cycle, the measured etch step of the MoS_2 was about 0.7 nm, which is a little thicker than the theoretical value of 0.65 nm. Previous investigations have shown that because of the trapping of H_2O on the SiO_2 substrate, the monolayer MoS_2 thickness may be slightly greater than the theoretical value;[30,31] therefore, we believe that one MoS_2 layer was completely etched after one ALET cycle. After the two cycles of ALET, as shown in Figure 6b, about 1.52 nm

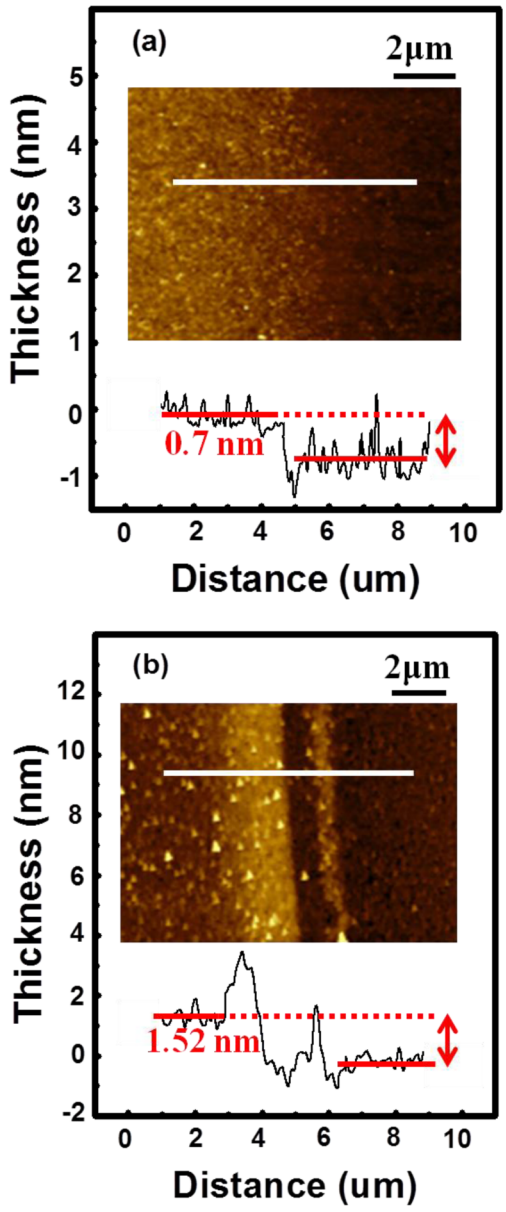

Figure 6. AFM step height (a) after one ALET cycle of one monolayer of MoS_2 and (b) after two ALET cycles of trilayer MoS_2. The MoS_2 was patterned with a photoresist, and the photoresist was removed after the ALET for the measurement of the step height using AFM. The big step heights at the boundary (two bright lines on the optical microscopic picture) are due to the photoresist residue remaining even after the photoresist removal to measure the etch step after two ALET cycles.

of etch depth, which is close to the thickness of two MoS_2 layers, was observed.

Figure 7 shows the narrow-scan XPS data of (a) Mo, (b) S, and (c) Cl that were measured during each step of the three cycles of ALET for the trilayer MoS_2. As shown in Figure 7a, the peaks at 229.5 and 232.6 eV that relate to the orbital binding energy of Mo $3d_{5/2}$ and Mo $3d_{3/2}$ were observed after the third Cl-adsorption step; but after the third desorption step, these peaks were removed and distorted. We believe that the remaining peak of Mo after the third Ar^+ ion-desorption step is related to the diffusion of the Mo into the SiO_2 or the oxidized Mo particle on the SiO_2, because the peak positions of the remaining Mo after the third Ar^+ ion-desorption step are

DOI: 10.1021/acsami.5b03491
ACS Appl. Mater. Interfaces 2015, 7, 15892−15897

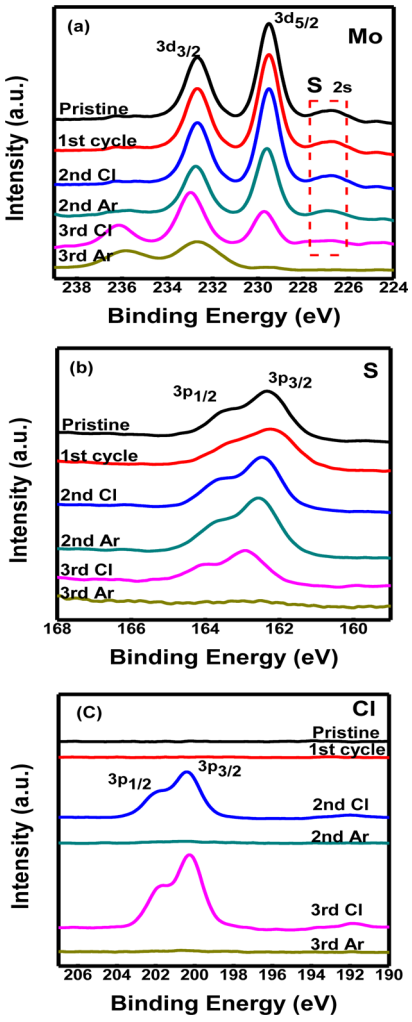

Figure 7. Narrow-scan XPS data of (a) Mo 3d, (b) S 2p, and (c) Cl 2p that were measured during each step of the three ALET cycles for the trilayer MoS_2.

exactly matched with those of the Mo $3d_{3/2}$ (236.3 eV) and Mo $3d_{5/2}$ (232.6 eV) that are related to MoO_3. Figure 7b shows the two peaks at 162.3 and 165.6 eV that are related to the binding energy of S $2p_{3/2}$ and S $2p_{1/2}$. These peaks are present throughout the third Cl-adsorption step but are not detected after the third Ar^+ exposure, indicating the complete removal of the third MoS_2 layer.[32] In the case of Cl, the large peak at 200.2 eV was only observed after the Cl-adsorption step; this peak was not detected after the Ar^+ ion-desorption step, indicating that the Cl adsorption on the MoS_2 during the radical-adsorption step was removed during the Ar^+ ion desorption. From the XPS results, the precise removal of one MoS_2 layer by one ALET cycle from the use of this method is therefore expected.

In the XPS narrow-scan data of Mo in Figure 7a, an additional peak at 227 eV is also shown and it remains until the Cl-adsorption step of the third ALET cycle. We found that this peak is related to the 2D MoS_2 structure, and when the 2D MoS_2 structure is damaged, the peak intensity decreased in addition to the emergence of an additional peak at 236 eV related to Mo^{6+} (see Figure S4). In the case of S, when the MoS_2 is damaged, the S $2p_{1/2}$ peak decreased (see Figure S4); however, as shown in Figure 7a and Figure 7b, the peak related to the 2D MoS_2 structure was not removed, and no peak related to the Mo^{6+} was observed until the Ar^+ ion-desorption step of the third ALET cycle. Also, a decrease of the S $2p_{1/2}$ peak was not found until the third ALET cycle. It is therefore believed that by using this ALET, a multilayer MoS_2 can be etched precisely layer-by-layer without noticeably damaging the exposed MoS_2 underlayer.

4. CONCLUSIONS

We have demonstrated that the thickness of a multilayer MoS_2 can be controlled layer-by-layer using Cl-radical adsorption and Ar^+ ion desorption in accordance with the ALET. Raman spectra, AFM data, and XPS data suggest that one monolayer of MoS_2 can be etched with one ALET cycle; therefore, the precise control of the etch layer can presumably be achieved using the ALET. Moreover, no Cl residue and no noticeable damage were found on the remaining MoS_2 underlayer after each ALET cycle. We believe that this ALET method can also be applicable when precisely controlling the layers of other 2D materials such as $MoSe_2$, WS_2, and BN; therefore, it can be utilized as a useful engineering tool for controlling the properties of next-generation 2D devices without inducing residue and damage.

■ ASSOCIATED CONTENT

Supporting Information

Figures showing CVD system, ICP system, microscope pictures and Raman spectra, and XPS data. The Supporting Information is available free of charge on the ACS Publications website at DOI: 10.1021/acsami.5b03491.

■ AUTHOR INFORMATION

Corresponding Authors

*G.Y.: e-mail, gyyeom@skku.edu.
*K.K.: e-mail, knam1004@skku.edu.

Notes

The authors declare no competing financial interest.

■ ACKNOWLEDGMENTS

This work was supported by SEMATECH through the SRC Project (2013-SE-2492) and also supported by Nano Material Technology Development Program through the National Research Foundation of Korea (NRF) funded by the Ministry of Education, Science and Technology (2012M3A7B4035323).

■ REFERENCES

(1) Tsukamoto, T.; Ogino, T. Control of Graphene Etching by Atomic Structures of the Supporting Substrate Surfaces. *J. Phys. Chem. C* **2011**, *115*, 8580−8585.
(2) Novoselov, K. S.; Geim, A. K.; Morozov, S. V.; Jiang, D.; Zhang, Y.; Dubonos, S. V.; Grigorieva, I. V.; Firsov, A. A. Electric Field Effect in Atomically Thin Carbon Films. *Science* **2004**, *306*, 666−669.
(3) Novoselov, K.; Geim, A. K.; Morozov, S.; Jiang, D.; Grigorieva, M. K. I.; Dubonos, S.; Firsov, A. Two-Dimensional Gas of Massless Dirac Fermions in Graphene. *Nature* **2005**, *438*, 197−200.
(4) Zhang, Y. B.; Tan, Y. W.; Stormer, H. L.; Kim, P. Experimental Observation of the Quantum Hall Effect and Berry's Phase in Graphene. *Nature* **2005**, *438*, 201−204.
(5) Tsukamoto, T.; Oqino, T. Morphology of Graphene on Step-Controlled Sapphire Surfaces. *Appl. Phys. Express* **2009**, *2*, 075502.
(6) Yang, S.; Li, Y.; Wang, X.; Huo, N.; Xia, J.; Li, S.; Li, J. High Performance Few-Layer GaS Photodetector and Its Unique Photo-Response in Different Gas Environments. *Nanoscale* **2014**, *6*, 2582−2587.

DOI: 10.1021/acsami.5b03491
ACS Appl. Mater. Interfaces 2015, 7, 15892−15897

(7) Yang, S.; Tongay, S.; Yue, Q.; Li, Y.; Li, B.; Lu, F. High-Performance Few-Layer Mo-Doped ReS_2 Nanosheet Photodetectors. *Sci. Rep.* **2014**, *4*, 5442.
(8) Lee, C.; Yan, H.; Brus, L.; Heinz, T.; Hone, J.; Ryu, S. Anomalous Lattice Vibrations of Single-and Few-Layer MoS_2. *ACS Nano* **2010**, *4* (5), 2695−2700.
(9) Li, B.; Yang, S.; Huo, N.; Li, Y.; Yang, J.; Li, R.; Fan, C.; Lu, F. Growth of Large Area Few-Layer or Monolayer MoS_2 from Controllable MoO_3 Nanowire Nuclei. *RSC Adv.* **2014**, *4*, 26407−26412.
(10) Yang, S.; Kang, J.; Yue, Q.; Yao, K. Vapor Phase Growth and Imaging Stacking Order of Bilayer Molybdenum Disulfide. *J. Phys. Chem. C* **2014**, *118*, 9203−9208.
(11) Huang, Y.; Wu, J.; Xu, X.; Ho, Y.; Ni, G.; Zou, Q.; Koon, G. K. W.; Zhao, W.; Neto, A.; Eda, G.; Shen, C.; Özyilmaz, B. An Innovative Way of Etching MoS_2: Characterization and Mechanistic Investigation. *Nano Res.* **2013**, *6*, 200−207.
(12) Brown, N.; Cui, N.; Mckinlev, A. An XPS Study of the Surface Modification of Natural MoS_2 Following Treatment in an RF-Oxygen Plasma. *Appl. Surf. Sci.* **1998**, *134*, 11−21.
(13) Radisavlievic, B.; Radenovic, A.; Brivio, J.; Giacometti, V.; Kis, A. Single-Layer MoS_2 Transistors. *Nat. Nanotechnol.* **2011**, *6*, 147−150.
(14) Welser, J.; Takaqi, S.-I.; Gibbons, J. F. Strain Dependence of the Performance Enhancement in Strained-Si n-MOSFETs. *IEDM Technical Digest*, International Electron Devices Meeting, San Francisco, CA, December 11−14, 1994; Institute of Electrical and Electronics Engineers: Piscataway, NJ, 1994; pp 373−376.
(15) Wu, J.; Li, H.; Yin, Z.; Li, H.; Liu, H.; Liu, J.; Cao, X.; Zhang, Q.; Zhang, H. Layer Thinning and Etching of Mechanically Exfoliated MoS_2 Nanosheets by Thermal Annealing in Air. *Small* **2013**, *19*, 3314−3319.
(16) Yin, Z.; Li, H.; Jiang, L.; Shi, Y.; Sun, Y.; Lu, G.; Zhang, Q.; Chen, X.; Zhang, H. Single-Layer MoS_2 Phototransistors. *ACS Nano* **2011**, *6*, 74−80.
(17) Zeng, Z.; Yin, Z.; Huang, X.; Li, H.; He, Q.; Lu, G.; Boev, F.; Zhang, H. Single-Layer Semiconducting Nanosheets: High-Yield Preparation and Device Fabrication. *Angew. Chem., Int. Ed.* **2011**, *50*, 11093−11097.
(18) Subhamov, G.; Atindra Nath, P.; Arindam, G. Nature of Electronic States in Atomically Thin MoS_2 Field-Effect Transistors. *ACS Nano* **2011**, *5*, 7707−7712.
(19) Fu, Y.; Feng, X.; Yan, M. F.; Wang, S. Y. First Principle Study on Electronic Structure and Optical Phonon Properties of 2H-MoS_2. *Physica B* **2013**, *426*, 103−107.
(20) Laura, G.; Juan, P.; Ruben, R.; Silvia, V. R.; Amelia, M. A.; Tascon, J. M. D. Production of Aqueous Dispersions of Inorganic Graphene Analogues by Exfoliation and Stabilization with Non-Ionic Surfactants. *RSC Adv.* **2014**, *4*, 14115−14127.
(21) Andres, C. G.; Maria, B.; Goossens, A. M.; Calado, V. E.; Zant, V. D.; Herre, S. J.; Steele, G. A. Laser-Thinning of MoS_2: On Demand Generation of a Single-Layer Semiconductor. *Nano Lett.* **2012**, *12*, 3187−3192.
(22) Yamamoto, M.; Einstein, T.; Fuhrer, M. S.; Cullen, W. G. Anisotropic Etching of Atomically Thin MoS_2. *J. Phys. Chem. C* **2013**, *117* (48), 25643−25649.
(23) Lim, W. S.; Kim, Y. Y.; Kim, H. K.; Jang, S.; Kwon, N. Y.; Park, B. J.; Ahn, J. H.; Chung, L.; Hong, B. H.; Yeom, G. Y. Atomic Layer Etching of Graphene for Full Graphene Device Fabrication. *Carbon* **2012**, *50*, 429−435.
(24) Min, K. S.; Kang, S. H.; Kim, J. K.; Jhon, M. S.; Yeom, G. Y. Atomic Layer Etching of Al_2O_3 using BCl_3 Ar for the Interface Passivation Layer of III−V MOS Devices. *Microelectron. Eng.* **2013**, *110*, 457−460.
(25) Kim, Y. Y.; Lim, W. S.; Park, J. B.; Yeom, G. Y. Layer by Layer Etching of the Highly Oriented Pyrolythic Graphite by Using Atomic Layer Etching. *J. Electrochem. Soc.* **2011**, *158*, D710−D714.
(26) Min, K. S.; Kang, S. H.; Kim, J. K.; Jhon, Y. I.; Hudnall, T. W.; Bielawski, C. W.; Banerjee, S. K.; Bersuker, G.; Jhon, M. S. Atomic Layer Etching of BeO Using BCl_3 Ar for the Interface Passivation Layer of III−V MOS Devices. *Microelectron. Eng.* **2014**, *114*, 121−125.
(27) Lim, W. S.; Park, J. B.; Park, B. J.; Yeom, G. Y. Low Damage Atomic Layer Etching of ZrO_2 by Using BCl_3 Gas and Ar Neutral Beam. *J. Nanosci. Nanotechnol.* **2009**, *9*, 7379−7382.
(28) Park, J. B.; Lim, W. S.; Park, B. J.; Park, I. H.; Kim, Y. W.; Yeom, G. Y. Atomic Layer Etching of Ultra-Thin HfO_2 Film for Gate Oxide in MOSFET Devices. *J. Phys. D* **2009**, *42*, 055202.
(29) Jhon, Y. I.; Min, K. S.; Yeom, G. Y.; Jhon, Y. M. Understanding Time-Resolved Processes in Atomic-Layer Etching of Ultra-Thin Al_2O_3 Film Using BCl_3 and Ar Neutral Beam. *Appl. Phys. Lett.* **2014**, *105*, 093104.
(30) Liu, Y. L.; Nan, H.; Wu, X.; Pan, W.; Wang, W.; Bai, J.; Zhao, W.; Sun, L.; Wang, X.; Ni, Z. Layer-by-Layer Thinning of MoS_2 by Plasma. *ACS Nano* **2013**, *7*, 4202−4209.
(31) Lee, H. C.; Lee, M. H.; Chung, C. W. Experimental Observation of the Transition from Nonlocal to Local Electron Kinetics in Inductively Coupled Plasmas. *Appl. Phys. Lett.* **2010**, *96*, 041503.
(32) Lee, Y. B.; Lee, J. H.; Bark, H.; Oh, I. K.; Ryu, G. H.; Lee, Z. H.; Kim, H. Q.; Cho, J. H.; Ahn, J. H.; Lee, C. G. Synthesis of Wafer-Scale Uniform Molybdenum Disulfide Films with Control over the Layer Number Using a Gas Phase Sulfur Precursor. *Nanoscale* **2014**, *6*, 2821−2826.

DOI: 10.1021/acsami.5b03491
ACS Appl. Mater. Interfaces 2015, 7, 15892−15897